

A DISSIPATIVE TIME REVERSAL TECHNIQUE FOR PHOTO-ACOUSTIC TOMOGRAPHY IN A CAVITY

LINH V. NGUYEN AND LEONID KUNYANSKY

ABSTRACT. We consider the inverse source problem arising in thermo- and photo- acoustic tomography. It consists in reconstructing the initial pressure from the boundary measurements of the acoustic wave. Our goal is to extend versatile time reversal techniques to the case of perfectly reflecting boundary of the domain. Standard time reversal works only if the solution of the direct problem decays in time, which does not happen in the setup we consider. We thus propose a novel time reversal technique with a non-standard boundary condition. The error induced by this time reversal technique satisfies the wave equation with a dissipative boundary condition and, therefore, decays in time. For larger measurement times, this method yields a close approximation; for smaller times, the first approximation can be iteratively refined, resulting in a convergent Neumann series for the approximation.

1. INTRODUCTION

We consider the inverse source problem arising in the thermo- and photoacoustic tomography (TAT and PAT) [Kru95, Kru99, Or64, XW06]. It consists in reconstructing the initial pressure in the acoustic wave from the values of time-dependent pressure measured on a surface, completely or partially surrounding the object of interest [KK08]. During the last decade, significant results were obtained in solving this problem under the assumption that the wave propagates in free space (see, for example [FPR04, Ku07a, Ku07b, Ng09, SU09, QSUZ11, AK07, FHR07, Nat12, XW05, Pa12, PS02, Ha09] and reviews [KK08, KK11, Sch11] for additional references). Applicability of the free space approximation depends on the type of the device(s) used to conduct the measurements: it is valid if reflection of waves from the detectors can be neglected. There are, however, a number of situations where this simple model is not applicable. For example, when the object is surrounded by glass plates optically scanned to measure the pressure, the waves experience multiple reflections as they would in a resonant cavity [CAB07, CB08, KHC13]. As a result, the assumption indispensable in the analysis of the classical TAT and PAT about the fast decrease of acoustic energy within the object, can no longer be made.

Thus, a novel approach is needed to solve the inverse source problem posed within a resonant cavity. The latter problem has attracted attention of analysts only recently. A particular case of a rectangular resonant cavity was considered in [CAB07, CB08, KHC13], and several solutions that exploit symmetries of such a geometry were proposed. In [HK15, SY15, AM15], more general acquisition geometries were considered; one of the main questions investigated in these papers is the applicability of various modifications of the time reversal algorithm to the problem under consideration.

Time reversal was successfully used by multiple authors, both theoretically and numerically, to solve the inverse source problem in the free space setting ([FPR04, HKN08, SU09, Hri09, QSUZ11, SU11, Hom13]). In the latter case, it consists in solving the wave equation backwards in time, within the domain Ω surrounded by the detectors, using the measured data to pose the Dirichlet boundary condition. In the simplest case of constant speed of sound $c(x) \equiv c_0$, the time reversal is initialized with zero conditions inside the domain (at time $t = T$ for sufficiently large T). Such approach works due to the fact that the solution of the direct problem in \mathbb{R}^3 with $c(x) \equiv c_0$ vanishes within the domain in a finite time $T_0(\Omega)$, due to the Huygens principle (and so time T is chosen to be greater or equal to $T_0(\Omega)$). In 2D and/or when $c(x)$ is not constant, more sophisticated methods are used to initialize time reversal [HKN08, SU09, QSUZ11]; however, all these techniques require a time decay of the solution of the direct problem.

The inverse source problem in a cavity with *partially* reflecting walls was solved in [AM15] using a time reversal approach. In this case, due to the outflow of energy through the boundary of the domain, solution of the direct problem still exhibits time decay, and, with some modifications, time

reversal can still be applied. A more difficult case is that of *perfectly* reflecting boundary (modeled by zero Neumann condition on the boundary). In this case, the direct problem is energy preserving, and acoustic oscillations in the cavity continue forever (here we neglect the effects of attenuation of waves in the tissues). This immediately makes classical time reversal inapplicable: the correct pressure and its time derivative inside the domain are unknown at any time. The error made when replacing these functions by any crude guess is not small. Under the standard Dirichlet boundary condition, this error does not decrease as t approaches 0.

Several attempts were made to modify the Dirichlet boundary condition so as to control this error. In [HK15], the boundary condition is multiplied by a smooth cut off function $\eta(t/T)$, where $\eta(\tau)$ vanishes at $\tau = 1$ with at least several derivatives. It was shown that under certain conditions on the eigenvalues of the Dirichlet and Neumann Laplacians on Ω , the approximate solutions corresponding to measurement time T converge to the correct one in the limit $T \rightarrow \infty$. However, for an arbitrary domain the aforementioned conditions on the eigenvalues are difficult to verify. In [SY15], the Dirichlet boundary condition was modified in such a way that the computed function is the result of averaging of a family of time-reversed solutions with different times T (“averaged time reversal”). The authors showed that, in the case of full boundary measurements, the operator that describes such a procedure is a contraction. Therefore, the result can be used either as a crude approximation, or a better solution can be computed by a converging Neumann series (involving multiple solutions of the direct problem and averaged time reversals). For the case when the data are available only on a part of the boundary (i.e. for the “partial data problem”), theoretical analysis was not completed; however, numerical experiments yielded successful reconstruction in this case, too. In [AM15], the problem with perfectly reflecting walls was considered mostly from a theoretical standpoint, and its unique solvability was proven under sufficiently general conditions.

In the present paper we propose a new time reversal technique in which the Dirichlet boundary condition is replaced by a non-standard boundary condition involving a linear combination of the normal- and time- derivatives of the solution (see equation (4)). While this new condition is satisfied by the solution of the direct problem, the error resulting from the time reversal satisfies the wave equation with dissipative boundary condition, and, thus, it decreases as time t approaches 0. We call this technique a “dissipative time reversal”. This method can be used either directly to obtain good approximations to the initial pressure (which converges exponentially as $T \rightarrow \infty$), or as a part of a Neumann series-based iterative algorithm.¹ In addition to being efficient numerically, our technique is relatively easy to analyze, allowing us to deliver an intuitive proof for the convergences in both full and partial data cases.

2. FORMULATION OF THE PROBLEM AND PRELIMINARIES

2.1. The direct problem. Let Ω be a domain in \mathbb{R}^d with smooth boundary $\partial\Omega$. In the realistic setup of PAT and TAT, the dimension d equals 3. However, we will consider any $d \geq 2$, for the sake of generality. We will denote by $\nu = \nu(x)$ the outward normal vector of $\partial\Omega$ at x . The speed of sound $c(x)$ is a positive, infinitely smooth function on \mathbb{R}^d .

For some positive time T , let us consider the following mixed boundary problem for the wave equation:

$$(1) \quad \begin{cases} u_{tt}(x, t) - c^2(x) \Delta u(x, t) = 0, & (x, t) \in \Omega \times (0, T], \\ \frac{\partial}{\partial \nu} u(x, t) = 0, & (x, t) \in \partial\Omega \times (0, T], \\ u(x, 0) = u_0(x), \quad u_t(x, 0) = u_1(x), & x \in \Omega, \end{cases}$$

where u_0 and u_1 are arbitrary functions with $u_0 \in H_0^1(\Omega)$, $u_1 \in L^2(\Omega)$. When $u_1 \equiv 0$ and $u_0(x)$ coincides with the initial pressure $f(x)$ in the tissues, the solution $u(x, t)$ of the above problem represents a model of TAT/PAT within a resonant cavity formed by the reflecting walls ([CAB07, CB08, KHC13]). In this case, one attempts to reconstruct initial pressure $f(x)$ from the measurements of $u(x, t)$ made on some subset of boundary $\partial\Omega$.

For convenience, we consider here a slightly more general problem, where both u_0 and u_1 are allowed to be non-zero. Let us assume that the values of pressure $u(x, t)$ are measured on a part Γ of the boundary

¹ Our idea of using the Neumann series-based iterative method is inspired by the influential paper [SU09]

$\partial\Omega$; we will consider both the case of full measurements when Γ coincides with $\partial\Omega$, and the case of partial data when Γ is an open proper subset of $\partial\Omega$. We will denote the measured data by $g(z, t)$:

$$(2) \quad g = u|_{\Gamma \times [0, T]}.$$

Our goal is to solve the following problem:

Problem 2.1. *Find the pair (u_0, u_1) from $g = u|_{\Gamma \times [0, T]}$. In other words, invert the map*

$$(3) \quad \Lambda_T : (u_0, u_1) \rightarrow g.$$

2.2. Our approach to the inverse problem. Let us fix a function $\lambda \in C^\infty(\partial\Omega)$ such that $\lambda > 0$ on Γ and $\lambda = 0$ on $\partial\Omega \setminus \bar{\Gamma}$. In addition, we will extend the data $g(z, t)$ to $\partial\Omega \setminus \bar{\Gamma} \times [0, T]$ by zero. The main idea of this paper is to find an approximation to u_0 and u_1 by solving the following time reversal problem

$$(4) \quad \begin{cases} v_{tt}(x, t) - c^2(x) \Delta v(x, t) = 0, & (x, t) \in \Omega \times [0, T], \\ \frac{\partial}{\partial \nu} v(x, t) - \lambda(x) v_t(x, t) = -\lambda(x) g_t(x, t), & (x, t) \in \partial\Omega \times [0, T], \\ v(x, T) = 0, \quad v_t(x, T) = 0, & x \in \Omega. \end{cases}$$

As we show below, for sufficiently large values of T , the functions $v(x, 0)$ and $v_t(x, 0)$ are good approximations to u_0 and u_1 , correspondingly.

In particular, in the context of the inverse problem of TAT/PAT with $u_1 = 0$ and $u_0 = f$, the function $v(x, 0)$ is a good approximation of $f(x)$. One can either use this approximation directly, or to realize an iterative refinement scheme converging to f and corresponding to a computation of a certain Neumann series.

The well-posedness of problem (4), validity of a so-obtained approximation and convergence of the Neumann series are the subject of the following sections. The starting point, however, is the analysis of the direct problem (1).

2.3. Properties of the direct problem. Let us define the space of pairs of functions \mathbb{H} as follows

$$\mathbb{H} := \{(u_0, u_1) | u_0 \in H^1(\Omega), u_1 \in L^2(\Omega)\},$$

where $H^1(\Omega)$ is the standard Sobolev space, with the norm defined, for an arbitrary function $h(x)$ by

$$\|h\|_{H^1(\Omega)}^2 \equiv \int_{\Omega} [h^2(x) + |\nabla h(x)|^2] dx = \|h\|_{L^2(\Omega)}^2 + \|\nabla h\|_{L^2(\Omega)}^2.$$

Then, \mathbb{H} is a Banach space under the norm $\|\cdot\|$ defined by

$$\|(u_0, u_1)\|^2 = \|u_0\|_{H^1(\Omega)}^2 + \|c^{-1}u_1\|_{L^2(\Omega)}^2.$$

For $(u_0, u_1) \in \mathbb{H}$, we define

$$\mathbb{E}(u_0, u_1) = \|\nabla u_0\|_{L^2(\Omega)}^2 + \|c^{-1}u_1\|_{L^2(\Omega)}^2,$$

and the semi-norm $|\cdot|$:

$$|(u_0, u_1)| = [\mathbb{E}(u_0, u_1)]^{1/2}.$$

It is well known that for any $(u_0, u_1) \in \mathbb{H}$ equation (1) has a unique solution u lying within the following class $\mathcal{K}(\Omega, T)$:

$$u \in \mathcal{K}(\Omega, T) \equiv \mathcal{C}([0, T]; H^1(\Omega)) \cap C^1([0, T]; L^2(\Omega)).$$

Therefore, Λ_T (defined by (3)) is a well-defined map from \mathbb{H} to $\mathcal{C}([0, T]; H^{1/2}(\partial\Omega))$.

3. WELL-POSEDNESS OF A MIXED BOUNDARY PROBLEM

Let $\lambda \in C^\infty(\partial\Omega)$. In this section, we study the following mixed boundary value problem:

$$(5) \quad \begin{cases} w_{tt}(x, t) - c^2(x) \Delta w(x, t) = 0, & (x, t) \in \Omega \times (0, T), \\ \frac{\partial}{\partial \nu} w(x, t) + \lambda(x) w_t(x, t) = h_t(x, t), & (x, t) \in \partial\Omega \times (0, T), \\ w(x, 0) = w_0(x), \quad w_t(x, 0) = w_1(x), & x \in \Omega. \end{cases}$$

Since this is not a standard problem, let us first define its weak solution. We will follow the spirit of [BLR92], where the weak (distributional) solution is defined for the case $h = 0$. For our purposes, it is sufficient to assume $(w_0, w_1) \in \mathbb{H}$ and $h \in \mathcal{C}([0, T]; H^{1/2}(\partial\Omega))$.

Definition 3.1. *Given $(w_0, w_1) \in \mathbb{H}$ and $h \in \mathcal{C}([0, T]; H^{1/2}(\partial\Omega))$, we say that $w \in \mathcal{D}'(\Omega \times (0, T))$ is a solution of (5) if the following equation holds for any test function $\psi \in \mathcal{D}(\Omega \times (0, T))$:*

$$(6) \quad \begin{aligned} \langle w, \psi \rangle = & - \iint_{\Omega \times [0, T]} c^{-2}(x) [w_0(x) \Psi_t(x, 0) - w_1(x) \Psi(x, 0)] dx + \int_{\partial\Omega} \lambda(x) w_0(x) \Psi(x, 0) dx \\ & - \iint_{\partial\Omega \times [0, T]} h(x, t) \Psi_t(x, t) dx dt - \int_{\partial\Omega} h(x, 0) \Psi(x, 0) dx. \end{aligned}$$

Here, Ψ is the solution of the dual problem

$$\begin{cases} c^{-2}(x) \Psi_{tt}(x, t) - \Delta \Psi(x, t) = \psi(x, t), & (x, t) \in \Omega \times (0, T), \\ \partial_\nu \Psi(x, t) - \lambda(x) \Psi_t(x, t) = 0, & (x, t) \in \partial\Omega \times (0, T), \\ \Psi(x, T) = 0, \quad \Psi_t(x, T) = 0, & x \in \Omega. \end{cases}$$

The uniqueness of solution w is obvious, since $\langle w, \psi \rangle$ is defined by the right hand side of (6) for all test functions ψ . The existence and regularity of this solution are more complicated. We only present here a partial result that is needed in the present paper:

Proposition 3.2. *Assume that $h = 0$ and $(w_0, w_1) \in \mathbb{H}$. Then, problem (5) has a unique solution*

$$w \in \mathcal{K}(\Omega, T).$$

Let us recall a result by [Ika70]. Assume that $h = 0$ and $(w_0, w_1) \in H^2(\Omega) \times H^1(\Omega)$ satisfies the compatibility condition

$$(7) \quad \frac{\partial}{\partial \nu} w_0 + \lambda(x) w_1 = 0, \quad \text{on } \partial\Omega.$$

Then, problem (5) has a unique solution

$$w \in \mathcal{C}([0, T]; H^2(\Omega)) \cap \mathcal{C}^1([0, T]; H^1(\Omega)) \cap \mathcal{C}^2([0, T]; L^2(\Omega)).$$

Proposition 3.2 can be proved by a simple approximation argument which we present here for the sake of completeness.

Proof of Proposition 3.2. It suffices to prove the existence part, since the uniqueness is trivial as mentioned above. Consider $(\varphi_0^n, \varphi_1^n) \in H^2(\Omega) \times H^1(\Omega)$ such that:

- 1) $(\varphi_0^n, \varphi_1^n) \rightarrow (w_0, w_1)$ in $H^1(\Omega) \times L^2(\Omega)$,
- 2) $\partial_\nu \varphi_0^n|_{\partial\Omega} = 0$ and $\varphi_1^n|_{\partial\Omega} = 0$.

Such a sequence $\{(\varphi_0^n, \varphi_1^n)\}$ always exists. For instance, we can choose φ_0^n to be a linear combination of eigenvectors of the Neumann Laplacian. Meanwhile, φ_1^n can be chosen as a linear combination of eigenvectors of the Dirichlet Laplacian.

Consider problem (5) with the initial condition $(\varphi_0^n, \varphi_1^n)$ (instead of (w_0, w_1)). Since $(\varphi_0^n, \varphi_1^n)$ satisfies the compatibility condition (7), problem (5) with such initial condition has a unique solution

$$w^n \in \mathcal{C}([0, T]; H^2(\Omega)) \cap \mathcal{C}^1([0, T]; H^1(\Omega)) \cap \mathcal{C}^2([0, T]; L^2(\Omega)).$$

Moreover, by simple integration by parts, we obtain for any $t_0 \in [0, T]$:

$$\mathbb{E}(w^n - w^m, t_0) + \int_{\partial\Omega \times [0, t_0]} \lambda(x) |w_t^n - w_t^m|^2 dx dt = \mathbb{E}(w^n - w^m, 0).$$

Therefore,

$$\mathbb{E}(w^n - w^m, t_0) \leq \mathbb{E}(w^n - w^m, 0).$$

We notice that

$$\mathbb{E}(w^n - w^m, 0) = \|\nabla(\varphi_0^n - \varphi_0^m)\|_{L^2(\Omega)}^2 + \|c^{-1}(\varphi_1^n - \varphi_1^m)\|_{L^2(\Omega)}^2 \rightarrow 0.$$

Since

$$\mathbb{E}(w^n - w^m, t) = \|\nabla(w^n(t, \cdot) - w^m(t, \cdot))\|^2 + \|c^{-1}(w_t^n(t, \cdot) - w_t^m(t, \cdot))\|^2,$$

we obtain $\{w^n\}$ is a Cauchy sequence in $\mathcal{C}([0, T]; H^1(\Omega))$ and $\{w_t^n\}$ is a Cauchy sequence in $\mathcal{C}([0, T]; L^2(\Omega))$. Therefore, there exists a function $w \in \mathcal{K}(\Omega, T)$ such that

$$\{w^n\} \rightarrow w \text{ in } \mathcal{C}([0, T], H^1(\Omega)), \quad \text{and } \{w_t^n\} \rightarrow w_t \text{ in } \mathcal{C}([0, T]; L^2(\Omega)).$$

It is easy to verify that w is a solution of problem (5), from the definition 3.1. This finishes our proof for the existence. \square

Let us apply the above result to the time reversal problem (4).

Proposition 3.3. *Problem (4) has a unique solution $v \in \mathcal{K}(\Omega, T)$.*

Proof. We first notice that problem (4) is the time reversed version of problem (5), considered in Section 3. The uniqueness of the solution follows trivially from the definition 3.1. We now prove the existence. Let us consider the following problem

$$(8) \quad \begin{cases} U_{tt}(x, t) - c^2(x) \Delta U(x, t) = 0, & (x, t) \in \Omega \times [0, T], \\ \frac{\partial}{\partial \nu} U(x, t) - \lambda(x) U_t(x, t) = 0, & (x, t) \in \partial\Omega \times [0, T], \\ U(x, T) = u(x, T), \quad U_t(x, T) = u_t(x, T), & x \in \Omega. \end{cases}$$

where $u(x, t)$ is the solution of the direct problem (1). Since $(u(\cdot, T), u_t(\cdot, T)) \in \mathbb{H}$, we obtain from Proposition 3.2 that the above problem has a (unique) solution $U \in \mathcal{K}(\Omega, T)$.

We notice that u also satisfies the boundary condition in problem (4).

Let $v = u - U$. It is easy to verify that v is a solution of (4). Moreover, from the regularity of u and U , we conclude that $v \in \mathcal{K}(\Omega, T)$. \square

4. SOLUTION OF THE INVERSE PROBLEM

4.1. Contraction properties of the time reversal operator. Similarly to [SY15, AM15], our analysis on the inversion of Λ relies on known results on stabilization of waves [BLR92]. For the sake of simplicity, we assume that all the geodesics of $(\mathbb{R}^3, c^{-2} dx^2)$ have finite contact order with the boundary $\partial\Omega$. Under this condition, the generalized bi-characteristics of the wave operator $\square = \partial_{tt} - c^2(x) \Delta$ on $\overline{\Omega}$ are uniquely defined (see, e.g., [BLR92]). Their projections on the physical space (i.e., $\overline{\Omega}$) are called the generalized rays.

Throughout the paper, we will assume that the following condition is satisfied:

Condition 4.1. *There is a finite value $T(\Omega, \Gamma) > 0$ such that every generalized ray of length $\geq T(\Omega, \Gamma)$ intersects Γ at one (or more) non-diffractive point(s).*

This is the **geometric control condition** (GCC), well known in control theory. We refer the reader to [BLR92] for a detailed discussion of GCC. This condition was shown in [SY15, AM15] to be sufficient for the stability of the inversion of Λ . Our results are also based on the assumption that GCC is satisfied.

Our work is based on the following fundamental result due to [BLR92]:

Proposition 4.2. *Consider problem (5) with $g = 0$. Assume that Condition 4.1 holds. Then, there is $\delta(T) < 1$ such that*

$$|(u(\cdot, T), u_t(\cdot, T))| \leq \delta(T) |(u_0, u_1)|.$$

Remark 4.3. *By applying Proposition 4.2 k times, one obtains*

$$|(u(\cdot, kT), u_t(\cdot, kT))| \leq \delta^k(T) |(u_0, u_1)|.$$

It is easy to conclude that $|(u(\cdot, T), u_t(\cdot, T))| \rightarrow 0$ exponentially as $T \rightarrow \infty$. That is, there are constant $C_1(\Omega)$ and $a > 0$ such that

$$|(u(\cdot, T), u_t(\cdot, T))| \leq C_1(\Omega) e^{-aT} |(u_0, u_1)|.$$

² The length here is understood in the metric $c^{-2} dx^2$. Condition 4.1 means that all the singularities of the solution of the wave equation (1) that start propagating at time 0, traveling along generalized bi-characteristics, reach the set Γ within the time interval $[0, T(\Omega, \Gamma)]$.

Given boundary data $g(x, t)$, we define the time reversal operator A through the solution $v(x, t)$ of the problem (4):

$$Ag = (v(., 0), v_t(., 0)).$$

Lemma 4.4. *Assume that condition 4.1 holds and $T \geq T(\Omega, \Gamma)$. Let I denote the identity map, then there is $\delta(T) < 1$ such that*

$$|(I - A\Lambda_T)(u_0, u_1)| \leq \delta(T)|(u_0, u_1)|, \quad \text{for all } (u_0, u_1) \in \mathbb{H}.$$

In other words, $I - A\Lambda_T$ is a contraction on \mathbb{H} under the semi norm $|\cdot|$.

Proof. Let $(u_0, u_1) \in \mathbb{H}$ and u be the solution of (1). We observe that

$$(I - A\Lambda_T)(u_0, u_1) = (U(., 0), U_t(., 0)),$$

where U is the solution of the problem (8).

Due to the well-known conservation of energy in the solution of the wave equation with Neumann boundary condition,

$$\mathbb{E}(u_0, u_1) = \mathbb{E}(u(., T), u_t(., T)),$$

or

$$|(u_0, u_1)| = |(u(., T), u_t(., T))|.$$

Due to Proposition 4.2,

$$|(U(., 0), U_t(., 0))| \leq \delta(T)|(u(., T), u_t(., T))|,$$

and the proof follows. \square

Remark 4.5. *Using Remark 4.3, instead of Proposition 4.2, in the above proof, we obtain that there exist constants $C_1(\Omega)$ and $a > 0$ such that*

$$|(I - A\Lambda_{kT})(u_0, u_1)| \leq C_1(\Omega)e^{-aT}|(u_0, u_1)|.$$

That is, the induced seminorm of $I - A\Lambda_T$ decreases exponentially as $T \rightarrow \infty$.

Lemma 4.4 describes the contraction property of our time reversal operator in the semi-norm $|\cdot|$. By itself, this result is not sufficient to prove the convergence under the norm $\|\cdot\|$. However, by restricting our attention to appropriate subspaces of \mathbb{H} , such a convergence can be attained. Indeed, let us consider the subspace \mathbb{H}_0 of \mathbb{H} defined by

$$\mathbb{H}_0 \equiv \left\{ \mathbf{h} = (h_0, h_1) \in \mathbb{H} \mid \int_{\partial\Omega} h_0 dx = 0 \right\},$$

and the subspace \mathbb{H}_1 of \mathbb{H}_0 consisting of pairs with the second component equal to zero:

$$\mathbb{H}_1 \equiv \{ \mathbf{h} = (h_0, 0) \in \mathbb{H}_0 \}.$$

Let us introduce two projectors Π_0 and Π_1 mapping the elements of \mathbb{H} into \mathbb{H}_0 and \mathbb{H}_1 , respectively:

$$\begin{aligned} \Pi_0 \mathbf{h} &\equiv \Pi_0(h_0, h_1) \equiv \left(h_0 - \frac{1}{|\partial\Omega|} \int_{\partial\Omega} h_0, h_1 \right), \\ \Pi_1 \mathbf{h} &\equiv \Pi_1(h_0, h_1) \equiv \left(h_0 - \frac{1}{|\partial\Omega|} \int_{\partial\Omega} h_0, 0 \right), \end{aligned}$$

where $|\partial\Omega|$ is the surface area of $\partial\Omega$. These projectors do not increase the semi-norm $|\cdot|$. That is,

$$|\Pi_0 \mathbf{h}| \leq |\mathbf{h}|, \quad |\Pi_1 \mathbf{h}| \leq |\mathbf{h}|.$$

Moreover, the subspaces \mathbb{H}_0 and \mathbb{H}_1 are invariant under compositions $\Pi_0(I - A\Lambda_T)$ and $\Pi_1(I - A\Lambda_T)$. In addition,

$$\begin{aligned} \Pi_0(I - A\Lambda_T) \mathbf{h} &= (I - \Pi_0 A\Lambda_T) \mathbf{h}, & \forall \mathbf{h} \in \mathbb{H}_0, \\ \Pi_1(I - A\Lambda_T) \mathbf{h} &= (I - \Pi_1 A\Lambda_T) \mathbf{h}, & \forall \mathbf{h} \in \mathbb{H}_1. \end{aligned}$$

Therefore, in accordance with Lemma 4.4, operators $(I - \Pi_0 A \Lambda_T)$ and $(I - \Pi_1 A \Lambda_T)$ are contractions in \mathbb{H}_0 and \mathbb{H}_1 correspondingly, under the seminorm $|\cdot|$:

$$(9) \quad |(I - \Pi_0 A \Lambda_T) \mathbf{h}| \leq |(I - A \Lambda_T) \mathbf{h}| \leq \delta(T) |\mathbf{h}|, \quad \forall \mathbf{h} \in \mathbb{H}_0,$$

$$(10) \quad |(I - \Pi_1 A \Lambda_T) \mathbf{h}| \leq |(I - A \Lambda_T) \mathbf{h}| \leq \delta(T) |\mathbf{h}|, \quad \forall \mathbf{h} \in \mathbb{H}_1.$$

Now we can invert operator Λ_T , restricted to \mathbb{H}_0 , by constructing converging Neumann series

$$\sum_{k=0}^{\infty} (I - \Pi_0 A \Lambda_T)^k \Pi_0 A \Lambda_T (u_0, u_1) = \sum_{k=0}^{\infty} (I - \Pi_0 A \Lambda_T)^k \Pi_0 A g.$$

Below we show that this series converges not only under the semi-norm $|\cdot|$ but also in the norm $\|\cdot\|$. In other words, we claim that the partial sums $\mathbf{u}^{(n)}$ of these series

$$(11) \quad \mathbf{u}^{(k)} = \sum_{j=0}^k (I - \Pi_0 A \Lambda_T)^j \Pi_0 A g$$

converge to $\mathbf{u} = (u_0, u_1)$ in the norm $\|\cdot\|$. These partial sums can be easily computed by the following iterative algorithm

$$(12) \quad \begin{aligned} \mathbf{u}^{(0)} &= 0, \\ \mathbf{u}^{(k+1)} &= (I - \Pi_0 A \Lambda_T) \mathbf{u}^{(k)} + \Pi_0 A g. \end{aligned}$$

The following theorem gives us a solution to Problem 2.1 by a Neumann series:

Theorem 4.6. *Suppose that condition 4.1 holds and the observation time T satisfies $T \geq T(\Omega, \Gamma)$. Then, the iterations $\mathbf{u}^{(k)}$ defined by (11) (or, equivalently, by (12)) converge to \mathbf{u} in norm $\|\cdot\|$, as follows:*

$$\|\mathbf{u} - \mathbf{u}^{(k)}\| \leq C_P(\Omega) \delta(T)^k \|\mathbf{u}\|, \quad \text{for all } \mathbf{u} \in \mathbb{H}_0,$$

with some constant $C_P(\Omega) > 1$ specified below.

To prove the above theorem, we will need the following generalization of the Poincare inequality.

Lemma 4.7. *There is a constant $C_P(\Omega) > 1$ such that for all $h \in H^1(\Omega)$ satisfying $\int_{\partial\Omega} h \, dx = 0$ the following inequality holds:*

$$\|h\|_{H^1(\Omega)} \leq C_P(\Omega) \|\nabla h\|_{L^2(\Omega)}.$$

Proof. Indeed, assume that the above statement is not true. Then, there exists a sequence $\{h_n\}_{n=1}^{\infty} \subset H^1(\Omega)$ such that

$$\|h_n\|_{L^2(\Omega)} = 1 \quad \text{and} \quad \lim_{n \rightarrow \infty} \|\nabla h_n\|_{L^2(\Omega)} = 0.$$

It follows that $\{h_n\}$ is bounded in $H^1(\Omega)$. Therefore, there is a weakly converging in $H^1(\Omega)$ subsequence $\{h_{n_k}\}_{k=1}^{\infty}$ and function $u \in H^1(\Omega)$, such that,

$$\begin{aligned} h_{n_k} &\rightarrow u \text{ strongly in } L^2(\Omega), \\ h_{n_k} &\rightarrow u \text{ weakly in } H^1(\Omega), \\ h_{n_k} &\rightarrow u \text{ weakly in } H^{1/2}(\partial\Omega). \end{aligned}$$

The limit u has the following three properties

$$\|u\|_{L^2(\Omega)} = 1, \quad \|\nabla u\|_{L^2(\Omega)} = 0, \quad \int_{\partial\Omega} u \, dx = 0.$$

The last two equations yield $u \equiv 0$, which contradicts to the first property $\|u\|_{L^2(\Omega)} = 1$, thus completing the proof. \square

Corollary 4.8. *There is a constant $C_P(\Omega) > 1$ (given by the above Lemma) such that the following inequality holds:*

$$(13) \quad |\mathbf{h}| \leq \|\mathbf{h}\| \leq C_P(\Omega) |\mathbf{h}|, \quad \text{for all } \mathbf{h} \in \mathbb{H}_0.$$

Proof of Theorem 4.6. By a simple induction argument applied to the recurrence relation (12) one obtains the following identity:

$$\mathbf{u} - \mathbf{u}^{(k)} = (I - \Pi_0 A \Lambda_T)^k \mathbf{u}, \quad k = 0, 1, 2, 3, \dots$$

Since $\mathbf{u} \in \mathbb{H}_0$, applying inequality (9) results in the following inequality

$$|\mathbf{u} - \mathbf{u}^{(k)}| \leq \delta(T)^k |\mathbf{u}|.$$

Further, using inequalities (13), one can transition to the following norm estimate

$$\|\mathbf{u} - \mathbf{u}^{(k)}\| \leq C_P(\Omega) \delta(T)^k \|\mathbf{u}\|,$$

thus, proving convergence of the Neumann series in the norm $\|\cdot\|$. \square

Remark 4.9. We note that, due to Remark 4.5,

$$(14) \quad \|\mathbf{u} - \Pi_0 A g\| \leq C_1(\Omega) C_P(\Omega) e^{-aT} \|\mathbf{u}\|.$$

Therefore, when T is sufficiently large, $\mathbf{u}^{(1)} = \Pi_0 A g$ is a good approximation to \mathbf{u} .

4.2. Inverse problem of TAT/PAT. The inverse problem of TAT/PAT is a particular case of Problem 2.1 with $u_0 = f$ and $u_1 = 0$. Therefore, f can be recovered from g by using the algorithm described in the previous section. However, the convergence can be accelerated and computations simplified by projecting computed approximations onto space \mathbb{H}_1 rather than \mathbb{H}_0 .

Let us introduce the notation $\mathbf{f} = (f, 0)$. The measured data g are still defined by equation (2) with $u(x, t)$ being a solution of the direct problem (1) with initial conditions

$$(u(0, x), u_t(0, x)) = \mathbf{f}(x).$$

We show below that the partial sums

$$\mathbf{u}^{(k)} = \sum_{j=0}^k (I - \Pi_1 A \Lambda_T)^j \Pi_1 A g;$$

of the following Neumann series converge to \mathbf{f} in norm $\|\cdot\|$. These sums are easy to compute using the following iterative relation

$$(15) \quad \begin{aligned} \mathbf{u}^{(0)} &= 0, \\ \mathbf{u}^{(k+1)} &= (I - \Pi_1 A \Lambda_T) \mathbf{u}^{(k)} + \Pi_1 A g. \end{aligned}$$

Theorem 4.10. Assume that the initial conditions of Problem 2.1 is given by $(u_0, u_1) = \mathbf{f}$. Suppose also condition 4.1 is satisfied and $T \geq T(\Omega, \Gamma)$. Then, iterations $\mathbf{u}^{(k)}$ defined by (11) (or, equivalently, by (12)) converge to \mathbf{f} in norm $\|\cdot\|$, as follows

$$\|\mathbf{f} - \mathbf{u}^{(k)}\| \leq C_P(\Omega) \delta(T)^k \|\mathbf{f}\|.$$

Proof. The proof is almost identical to that of Theorem 4.6, with inequality (10) used instead of (9). \square

Remark 4.11. Similarly to Remark 4.9,

$$\|\mathbf{f} - \Pi_1 A g\| \leq C_1(\Omega) C_P(\Omega) e^{-aT} \|\mathbf{f}\|,$$

and, when T is sufficiently large, $\mathbf{u}^{(1)} = \Pi_1 A g$ is a good approximation to \mathbf{f} .

5. NUMERICAL IMPLEMENTATION AND SIMULATIONS

5.1. Implementation. One of the advantages of the present method is the ease of implementation using standard finite differences. Unlike algorithms of [SY15], our approach does not require solving the Dirichlet problem for Laplace equation to initialize the time reversal. (The latter problem is well studied and various methods for its solution are known. However, efficient numerical schemes for arbitrary domains are quite sophisticated and require noticeable effort to implement).

Our numerical realization of the algorithm is based on equation (15) that requires computing operators Λ_T and A . These operators represent solutions of the wave equation forward and backwards in time, respectively; they were calculated using finite difference stencils as described below.

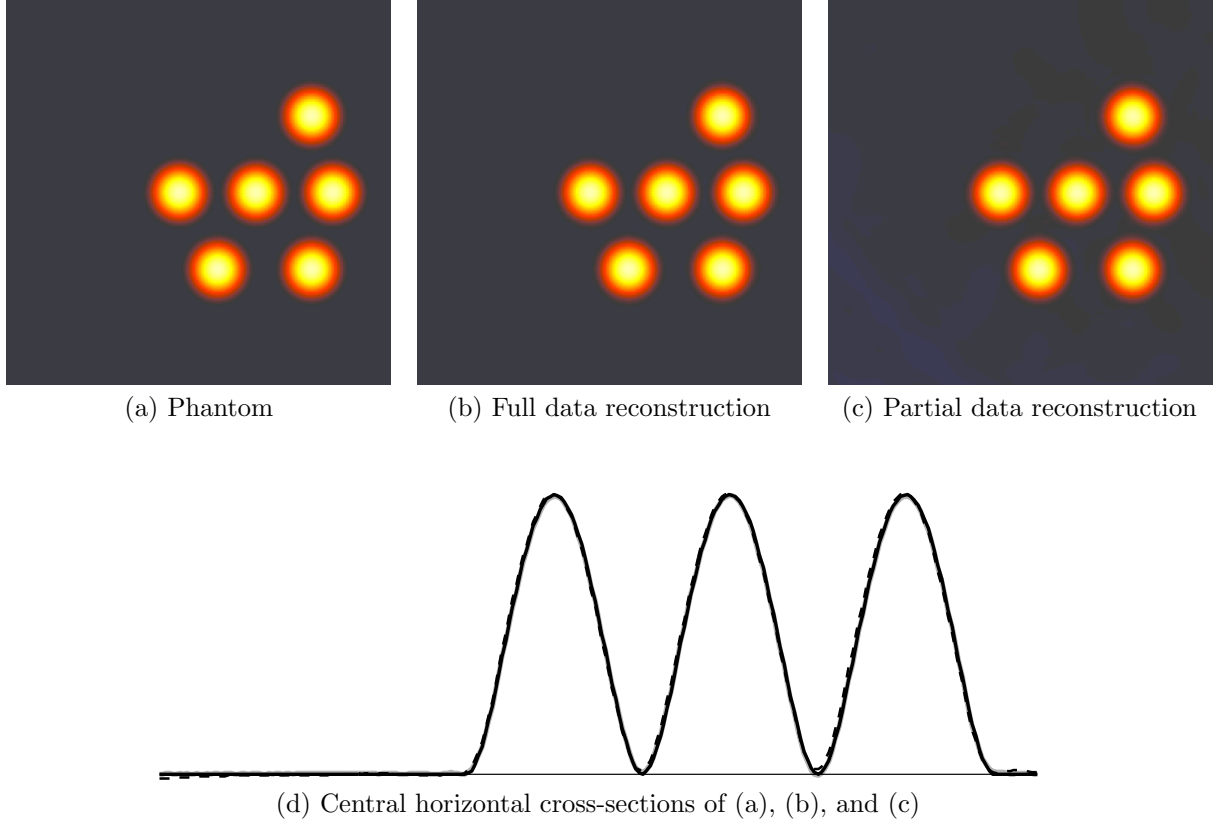


FIGURE 1. Reconstruction with $T = 5$. In (d): gray line represents the phantom, dashed line shows image reconstructed from the partial data, black line shows full data reconstruction

Our simulations were performed on a 2D square domain $[-1, 1] \times [-1, 1]$. Throughout this section we will represent our 2D spatial variable x in the coordinate form, and will change the notations for all functions correspondingly:

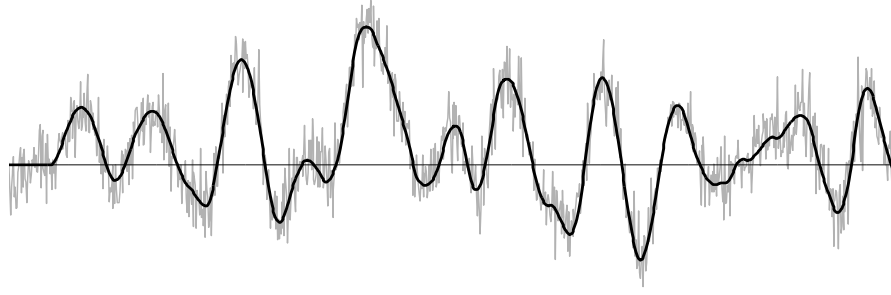
$$x = (\mathbf{x}, \mathbf{y}), \quad u(x, t) = u(\mathbf{x}, \mathbf{y}, t), \quad v(x, t) = v(\mathbf{x}, \mathbf{y}, t), \quad \text{etc.}$$

Our square domain was discretized using Cartesian grid of size 257×257 , with the step $\Delta x = \Delta y = 2/257$; time was discretized uniformly with the step $\Delta t = 0.5\Delta x$. The speed of sound $c(\mathbf{x}, \mathbf{y})$ was set to 1, for simplicity. Time stepping inside the domain in the forward direction was implemented by applying standard second-order centered stencils in both time and space to the discretized solution $u(\mathbf{x}_k, \mathbf{y}_l, t_j)$

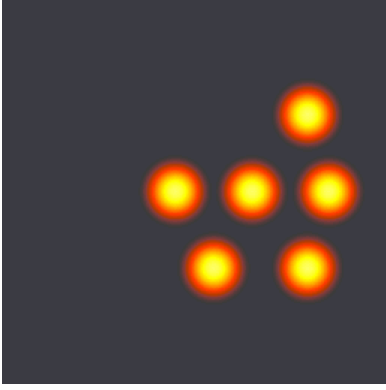
$$\begin{aligned} \frac{\partial^2}{\partial x^2} u(\mathbf{x}_k, \mathbf{y}_l, t_j) &\approx \frac{\partial^2}{\partial x^2} \widetilde{u(\mathbf{x}_k, \mathbf{y}_l, t_j)} \equiv \frac{u(\mathbf{x}_{k+1}, \mathbf{y}_l, t_j) + u(\mathbf{x}_{k-1}, \mathbf{y}_l, t_j) - 2u(\mathbf{x}_k, \mathbf{y}_l, t_j)}{\Delta x^2}, \\ \frac{\partial^2}{\partial y^2} u(\mathbf{x}_k, \mathbf{y}_l, t_j) &\approx \frac{\partial^2}{\partial y^2} \widetilde{u(\mathbf{x}_k, \mathbf{y}_l, t_j)} \equiv \frac{u(\mathbf{x}_k, \mathbf{y}_{l+1}, t_j) + u(\mathbf{x}_k, \mathbf{y}_{l-1}, t_j) - 2u(\mathbf{x}_k, \mathbf{y}_l, t_j)}{\Delta y^2}, \\ \frac{\partial^2}{\partial t^2} u(\mathbf{x}_k, \mathbf{y}_l, t_j) &\approx \frac{\partial^2}{\partial t^2} \widetilde{u(\mathbf{x}_k, \mathbf{y}_l, t_j)} \equiv \frac{u(\mathbf{x}_k, \mathbf{y}_l, t_{j+1}) + u(\mathbf{x}_k, \mathbf{y}_l, t_{j-1}) - 2u(\mathbf{x}_k, \mathbf{y}_l, t_j)}{\Delta t^2}, \end{aligned}$$

resulting in the formula

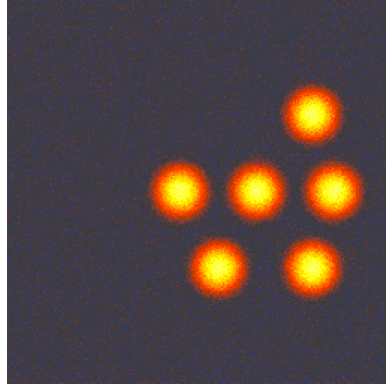
$$u(\mathbf{x}_k, \mathbf{y}_l, t_{j+1}) = 2u(\mathbf{x}_k, \mathbf{y}_l, t_j) - u(\mathbf{x}_k, \mathbf{y}_l, t_{j-1}) + \Delta t^2 \left(\frac{\partial^2}{\partial x^2} \widetilde{u(\mathbf{x}_k, \mathbf{y}_l, t_j)} + \frac{\partial^2}{\partial y^2} \widetilde{u(\mathbf{x}_k, \mathbf{y}_l, t_j)} \right),$$



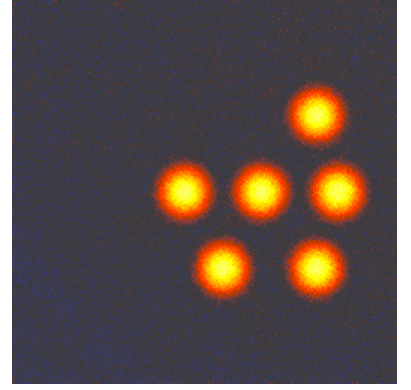
(a) Exact data $g(x, t)$ and data with added 50% noise (in L^2 norm), for one x



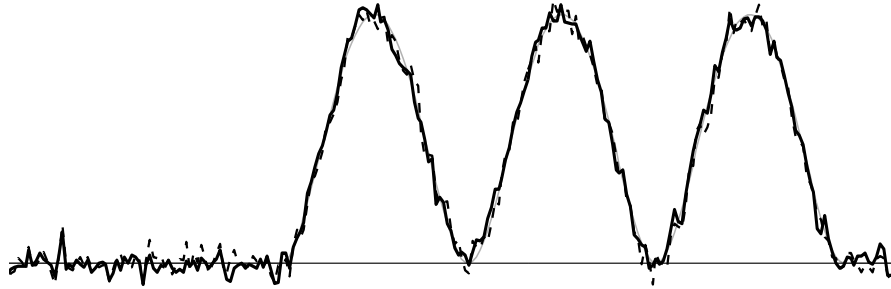
(b) Phantom



(c) Full data reconstruction



(d) Partial data reconstruction



(e) Central horizontal cross-sections of (b), (c), and (d)

FIGURE 2. Reconstruction with $T = 5$ and with added 50% noise (in L^2 norm). In (e): gray line represents the phantom, dashed line shows image reconstructed from the partial data, black line shows full data reconstruction

where tilde denotes approximate quantities. Time stepping backwards in time (when computing A) were done similarly

$$(16) \quad v(\mathbf{x}_k, \mathbf{y}_l, t_{j-1}) = 2v(\mathbf{x}_k, \mathbf{y}_l, t_j) - v(\mathbf{x}_k, \mathbf{y}_l, t_{j+1}) + \Delta t^2 \left(\widetilde{\frac{\partial^2}{\partial \mathbf{x}^2} v(\mathbf{x}_k, \mathbf{y}_l, t_j)} + \widetilde{\frac{\partial^2}{\partial \mathbf{y}^2} v(\mathbf{x}_k, \mathbf{y}_l, t_j)} \right).$$

When computing action of the operator Λ_T (forward problem), the Neumann boundary condition was represented by the simplest first-order two-point stencil; this results in the values at the boundary points being set to the values of the nearest grid points.

The discretization of the non-standard boundary condition

$$(17) \quad \frac{\partial}{\partial \nu} v(x, t) - \lambda(x) \frac{\partial}{\partial t} v(x, t) = -\lambda(x) \frac{\partial}{\partial t} g(x, t),$$

arising in problem (4) was performed as follows. The simplest first-order two-point forward stencils were used to approximate all the derivatives; for example $\frac{\partial}{\partial t} v$ was approximated at $t = t_{j-1}$, $\mathbf{x} = \mathbf{x}_0$ by

$$\frac{\partial}{\partial t} v(\mathbf{x}_0, \mathbf{y}_l, t_{j-1}) \approx \frac{\partial}{\partial t} \widetilde{v(\mathbf{x}_0, \mathbf{y}_l, t_{j-1})} \equiv \frac{v(\mathbf{x}_0, \mathbf{y}_l, t_j) - v(\mathbf{x}_0, \mathbf{y}_l, t_{j-1})}{\Delta t},$$

and $\frac{\partial}{\partial t} g$ was computed similarly. The normal derivative was also approximated by the simplest two-point stencil applied to values at time t_{j-1} ; for example, on the side with $\mathbf{x} = \mathbf{x}_0$ the following formula was used:

$$\frac{\partial}{\partial \nu} v(\mathbf{x}_0, \mathbf{y}_l, t_{j-1}) = -\frac{\partial}{\partial \mathbf{x}} v(\mathbf{x}_0, \mathbf{y}_l, t_{j-1}) \approx -\frac{\partial}{\partial \mathbf{x}} \widetilde{v(\mathbf{x}_0, \mathbf{y}_l, t_{j-1})} \equiv -\frac{v(\mathbf{x}_1, \mathbf{y}_l, t_{j-1}) - v(\mathbf{x}_0, \mathbf{y}_l, t_{j-1})}{\Delta \mathbf{x}}.$$

Substituting the last two equations into (17) resulted in

$$\frac{v(\mathbf{x}_0, \mathbf{y}_l, t_{j-1}) - v(\mathbf{x}_1, \mathbf{y}_l, t_{j-1})}{\Delta \mathbf{x}} = \frac{\lambda(\mathbf{x}_0, \mathbf{y}_l)}{\Delta t} [v(\mathbf{x}_0, \mathbf{y}_l, t_j) - v(\mathbf{x}_0, \mathbf{y}_l, t_{j-1}) - g(\mathbf{x}_0, \mathbf{y}_l, t_j) + g(\mathbf{x}_0, \mathbf{y}_l, t_{j-1})]$$

or

$$(18) \quad v(\mathbf{x}_0, \mathbf{y}_l, t_{j-1}) = v(\mathbf{x}_1, \mathbf{y}_l, t_{j-1}) + \gamma(\mathbf{x}_0, \mathbf{y}_l) [v(\mathbf{x}_0, \mathbf{y}_l, t_j) - v(\mathbf{x}_0, \mathbf{y}_l, t_{j-1}) - g(\mathbf{x}_0, \mathbf{y}_l, t_j) + g(\mathbf{x}_0, \mathbf{y}_l, t_{j-1})],$$

where

$$\gamma(\mathbf{x}_0, \mathbf{y}_l) \equiv \frac{\lambda(\mathbf{x}_0, \mathbf{y}_l) \Delta \mathbf{x}}{\Delta t}.$$

Solving (18) for $v(\mathbf{x}_0, \mathbf{y}_l, t_{j-1})$ yielded

$$(19) \quad v(\mathbf{x}_0, \mathbf{y}_l, t_{j-1}) = \frac{v(\mathbf{x}_1, \mathbf{y}_l, t_{j-1})}{1 + \gamma(\mathbf{x}_0, \mathbf{y}_l)} + \frac{\gamma(\mathbf{x}_0, \mathbf{y}_l) [v(\mathbf{x}_0, \mathbf{y}_l, t_j) - g(\mathbf{x}_0, \mathbf{y}_l, t_j) + g(\mathbf{x}_0, \mathbf{y}_l, t_{j-1})]}{1 + \gamma(\mathbf{x}_0, \mathbf{y}_l)}.$$

Approximation of boundary condition (17) on other parts of the boundary was done similarly. In order to apply (19) (and similar expression on the other parts of the boundary), one first applies (16) at all discretization points inside of the computational domain. Then (19) is fully defined.

In the absence of experimentally measured data, in order to validate the reconstruction algorithm one needs to simulate values of $g(x, t)$ on Γ . One could use the finite difference algorithm described above to approximately compute $g(x, t)$ for a chosen phantom $\mathbf{f} = (f, 0)$. However, doing so would constitute the so-called “inverse crime”: sometimes simulations will produce inordinately good reconstructions due to the spurious cancellation of errors if the forward and direct problems are solved using the same discretization techniques. Thus, in order to compute g we utilized the following method based on separation of variables. Function f was expanded in the orthogonal series of eigenfunctions $\varphi_{k,l}$ of the Neumann Laplacian on our square domain

$$\begin{aligned} f(\mathbf{x}, \mathbf{y}) &= \sum_{k,l} c_{k,l} \varphi_{k,l}(\mathbf{x}, \mathbf{y}), \\ \varphi_{k,l}(\mathbf{x}, \mathbf{y}) &= \cos(k\bar{\mathbf{x}}) \cos(l\bar{\mathbf{y}}), \quad k = 0, 1, 2, \dots, \quad l = 0, 1, 2, \dots, \\ \bar{\mathbf{x}} &= \pi(\mathbf{x} + 1)/2, \quad \bar{\mathbf{y}} = \pi(\mathbf{y} + 1)/2. \end{aligned}$$

This was done efficiently using the 2D Fast Cosine Fourier transform algorithm (FCT). Then, solution of the forward problem was computed as the series

$$u(\mathbf{x}, \mathbf{y}, t) = \sum_{k,l} c_{k,l} \varphi_{k,l}(\mathbf{x}, \mathbf{y}) \cos(\lambda_{k,l} t), \quad \lambda_{k,l} = \frac{\pi}{2} \sqrt{k^2 + l^2}, \quad k, l = 0, 1, 2, \dots$$

For each value of t , the above 2D cosine series were also summed using the FCT. The resulting algorithm is quite fast, and, more importantly, it is spectrally accurate with respect to f . If f has high degree of smoothness, this series solution yields much higher accuracy than the finite difference techniques we utilized as parts of the reconstruction algorithm.

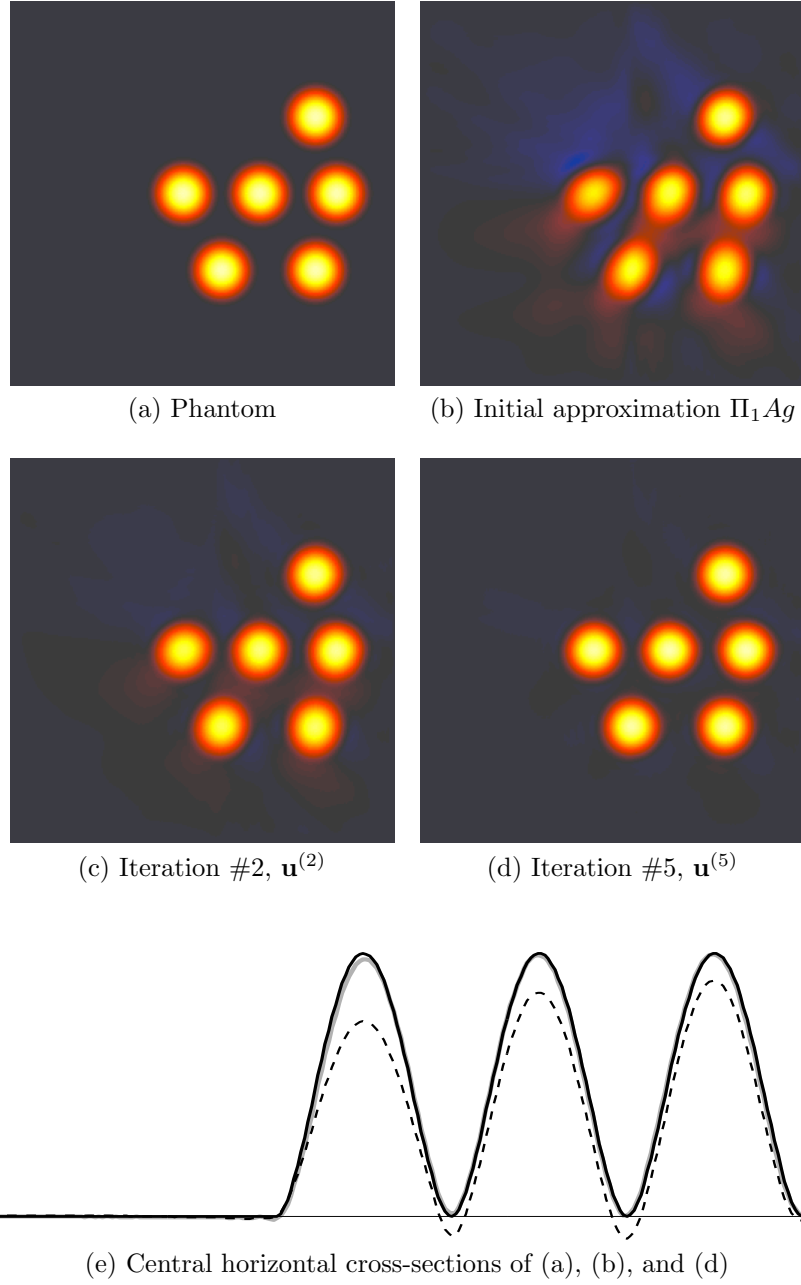


FIGURE 3. Reconstruction from the full boundary data, $T = 1.6$. In (e): gray line is the phantom, dashed line shows the initial approximation, black line presents iteration #5

5.2. Simulations. We conducted several numerical experiments to verify theoretical conclusions of previous sections. Two acquisition schemes were considered: a full data scheme with $g(x, t)$ given on all sides of the square domain, and a partial data scheme with g known only on the left and bottom sides of the square. Since we assumed $c(x) \equiv 1$, $T(\Omega, \Gamma)$ equals $2\sqrt{2}$ in the former case (i.e., the length of the diagonal of the square) and $4\sqrt{2}$ in the latter case. Experimentally, we found that these times are too pessimistic, and a half of that time is quite enough for the reconstruction. This implies that our theoretical results may be not sharp. Although we were not able to improve these theoretical estimates, we present below simulations with the measurement times significantly reduced compared to $T(\Omega, \Gamma)$.

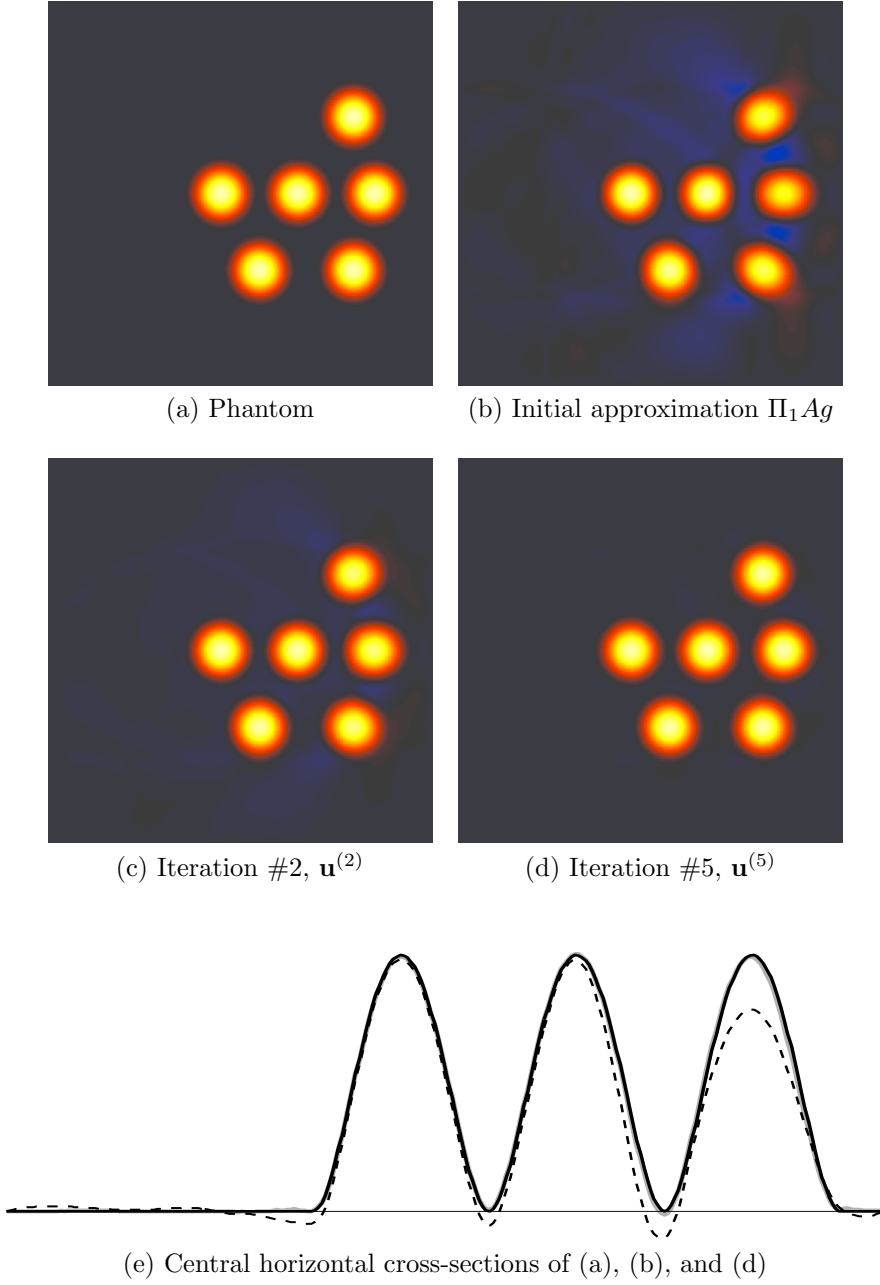


FIGURE 4. Reconstruction from the data given at the left and bottom sides of the square domain, $T = 3$. In (e): gray line is the phantom, dashed line represents the initial approximation, black line shows iteration #5

As a phantom, we utilized a sum of six shifted finitely supported $C^1(\Omega)$ functions of the radial variable, shown as a color-scale image in Figure 1(a). Such a smooth phantom reduces errors related to finite difference computations and allows us to concentrate on convergence of the algorithm per se.

The goal of our first two simulations was to see how well the initial approximation $\Pi_1 Ag$ can approximate f . To this end the measurement time T was chosen to equal to 5; this corresponds to the time of two and a half bounces of waves between the opposite sides of the domain. Reconstruction from full data is shown in Figure 1(b) and partial data reconstruction is presented in Figure 1(c). Image in Figure 1(d) demonstrates profiles of the central horizontal cross sections of the three previous images,

with the phantom represented by a gray line, full time reconstruction shown as a black line, and partial data image drawn with a dashed line. The full data image is practically perfect; the corresponding black line in Figure 1(d) lying on top of the gray line, rendering the latter almost invisible. The relative $L^2(\Omega)$ reconstruction error equals 1.1% in the image of Figure 1(b). The partial data reconstruction is just slightly less accurate, with the relative $L^2(\Omega)$ error equal to 6.8%. In any reconstruction from real data such error would be negligible compared to errors introduced by imperfections of real data.

In order to illustrate the low sensitivity of the algorithm to the noise in the data, we repeated the previous simulation with the data contaminated by 50% white noise (in the relative L^2 norm). As in the first simulation, only the initial guess $\Pi_1 Ag$ was computed, without the successive iterative refinement. Figure 2(a) shows the time series representing $g(x, t)$ for one of the points x , with and without added noise. Figure 2(b)-(d) demonstrate the same phantom, and the full and partial data reconstructions, respectively. The errors in the two reconstructions were of about the same order, 19% and 22% in the relative $L^2(\Omega)$ norm, with the partial data giving, for some reason, slightly better result in this norm. The central cross sections of these images are shown in Figure 2(e).

Our remaining two simulations were intended to verify the convergence of the algorithm in the case when measurement time T is close to a half of $T(\Omega, \Gamma)$. Figures 3(a)-(e) demonstrate results of a full data reconstruction with T equal to 1.6 (compare to $T(\Omega, \Gamma) = 2\sqrt{2} \approx 2.828$). Figures 3(a)-(d) show the phantom, the first approximation $\Pi_1 Ag$, and the second and the fifth iterations ($\mathbf{u}^{(2)}$ and $\mathbf{u}^{(5)}$), respectively. Figure 3(e) presents central horizontal cross-sections of the phantom, the first approximation $\Pi_1 Ag$, and of the fifth iterations. One can notice that, while the initial approximation had been noticeably distorted, the fifth iteration yields a close approximation to $f(x)$. The relative $L^2(\Omega)$ norm of the error in $\mathbf{u}^{(5)}$ was 3.3%.

The final series of images in Figure 4 demonstrates the results of the reconstruction from the partial data, with T equal to 3 (compare to $T(\Omega, \Gamma) = 4\sqrt{2} \approx 5.6569$). As before, the phantom, the initial approximation, and the second and the fifth iterations are shown in Figure 4(a)-(d), respectively. Figure 4(e) presents the central horizontal cross sections of images in Figure 4(a), (b), and (d). The relative $L^2(\Omega)$ error in the fifth iteration $\mathbf{u}^{(5)}$ was 5.4%; for most practical purposes this would be more than acceptable.

6. CONCLUSIONS

We presented a novel dissipative time reversal approach for solving the inverse source problem of TAT/PAT posed within a cavity with perfectly reflecting walls. Unlike the previous work of [HK15, SY15] where Dirichlet boundary condition was used, we utilize the non-standard boundary condition (4). The latter leads to the dissipative boundary condition (8) imposed on the error $U(x, t)$, and, hence, to a natural decay of $U(x, 0)$ with the growth of T . Our approach results in two reconstruction methods: i) a non-iterative approximation, converging exponentially to f as $T \rightarrow \infty$, and ii) a Neumann series formula. These two algorithms are applicable for both full and partial data problems.

Compared to [HK15], where rather stringent conditions on the eigenvalues of the Neumann and Dirichlet Laplacians on Ω are required for convergence, our approach is based on the much less restrictive GCC (Condition 4.1). Moreover, unlike the method of [SY15], our technique does not require computing the harmonic extension of the boundary values, which significantly simplifies its numerical realization. It should be noted that the requirement $T \geq T(\Omega, \Gamma)$ is sharp for the convergence in Theorem 4.6 (dealing with the general Problem 2.1). However, it is not sharp for the convergence in Theorem 4.10 (dealing with the inverse problem of TAT/PAT). Specifically, for the case of the full data, it is twice of the sharp time for the convergence of the TAT/PAT's inverse problem, obtained in [SY15]. Nevertheless, our numerical simulations show that the present algorithm performs very well with such sharp measurement times.

While we only considered the simplest wave equation in the Euclidean spaces, our analysis can be extended to problems formulated on Riemannian manifolds (as in [SY15]) and/or to problems with a potential (as in [AM15]).

ACKNOWLEDGMENT

The first author is grateful to C. Bardos, G. Nakamura, and P. Stefanov for helpful discussions and comments. The second author thanks L. Friedlander for a helpful discussion. The first and second authors were partially supported by the NSF/DMS awards # 1212125 and 1211521, respectively.

REFERENCES

- [AK07] M. Agranovsky and P. Kuchment, Uniqueness of reconstruction and an inversion procedure for thermoacoustic and photoacoustic tomography with variable sound speed, *Inverse Problems* **23** (2007) 2089–102.
- [AM15] S. Acosta and C. Montalto. Multiwave imaging in an enclosure with variable wave speed. *Inverse Problems*, 31(6):065009, 2015.
- [BLR92] C. Bardos, G. Lebeau, and J. Rauch. Sharp sufficient conditions for the observation, control, and stabilization of waves from the boundary. *SIAM J. Control Optim.*, 30(5):1024–1065, 1992.
- [CAB07] B. Cox, S. Arridge, and P. Beard. Photoacoustic tomography with a limited-aperture planar sensor and a reverberant cavity. *Inverse Problems*, 23(6):S95, 2007.
- [CB08] B. Cox and P. Beard. Photoacoustic tomography with a single detector in a reverberant cavity. *The Journal of the Acoustical Society of America*, 123(5):3371–3371, 2008.
- [Ell14] R. Ellwood, E. Zhang, P. Beard and B. Cox 2014 Photoacoustic imaging using acoustic reflectors to enhance planar arrays, *J. Biomed. Opt.* **19** 126012.
- [FPR04] D. Finch, S. Patch, and Rakesh. Determining a function from its mean values over a family of spheres. *SIAM J. Math. Anal.*, 35(5):1213–1240 (electronic), 2004.
- [FHR07] D. Finch, M. Haltmeier and Rakesh 2007 Inversion of spherical means and the wave equation in even dimensions *SIAM J. Appl. Math.* **68**(2) 392–412
- [Ha09] M. Haltmeier, Frequency domain reconstruction in photo- and thermoacoustic tomography with line detectors *Math. Models Methods Appl. Sci.* **19**(2): 283–306, 2009
- [HK15] B. Holman and L. Kunyansky. Gradual time reversal in thermo- and photo-acoustic tomography within a resonant cavity. *Inverse Problems*, 31(3):035008, 2015.
- [HKN08] Y. Hristova, P. Kuchment, and L. Nguyen. Reconstruction and time reversal in thermoacoustic tomography in acoustically homogeneous and inhomogeneous media. *Inverse Problems*, 24(5):055006, 25, 2008.
- [Hom13] A. Homan. Multi-wave imaging in attenuating media. *Inverse Problems and Imaging*, 7(4):1235–1250, 2013.
- [Hri09] Y. Hristova. Time reversal in thermoacoustic tomography—an error estimate. *Inverse Problems*, 25(5):055008, 14, 2009.
- [Ika70] M. Ikawa. On the mixed problem for hyperbolic equations of second order with the neumann boundary condition. *Osaka Journal of Mathematics*, 7(1):203–223, 1970.
- [Kru95] R. Kruger, P. Liu, Y. Fang and C. Appledorn 1995 Photoacoustic ultrasound (PAUS) reconstruction tomography *Med. Phys.* **22** 1605–09
- [Kru99] R. Kruger, D. Reinecke, and G. Kruger 1999 Thermoacoustic computed tomography - technical considerations *Med. Phys.* **26** 1832–7
- [KHC13] L. Kunyansky, B. Holman, and B. Cox. Photoacoustic tomography in a rectangular reflecting cavity. *Inverse Problems*, 29(12):125010, 20, 2013.
- [KK08] P. Kuchment and L. Kunyansky. Mathematics of thermoacoustic tomography. *European J. Appl. Math.*, 19(2):191–224, 2008.
- [KK11] P. Kuchment and L. Kunyansky, Mathematics of Photoacoustic and Thermoacoustic Tomography, Chapter 19, *Handbook of Mathematical Methods in Imaging*, Springer-Verlag, (2011) 819–865.
- [Ku07a] L. Kunyansky, Explicit inversion formulae for the spherical mean Radon transform, *Inverse Problems*, **23** (2007) 737–783.
- [Ku07b] L. Kunyansky, A series solution and a fast algorithm for the inversion of the spherical mean Radon transform, *Inverse Problems*, **23** (2007) S11–S20.
- [Nat12] F. Natterer 2012 Photo-acoustic inversion in convex domains *Inverse Problems Imaging* **6** 315–20
- [Ng09] L. Nguyen, A family of inversion formulas in thermoacoustic tomography, *Inverse Problems and Imaging*, **3** (2009) 649–675.
- [Or64] A. Oraevsky, S. Jacques, R. Esenaliev and F. Tittel 1994 Laser-based optoacoustic imaging in biological tissues *Proc. SPIE* **2134A** 122–8
- [Pa12] V. Palamodov 2012 A uniform reconstruction formula in integral geometry *Inverse Problems* **28** 065014
- [PS02] D. Popov and D. Sushko 2002 A parametrix for the problem of optical-acoustic tomography *Doklady Mathematics* **65** (1) 19–21
- [QSUZ11] J. Qian, P. Stefanov, G. Uhlmann, and H. Zhao. An efficient Neumann series-based algorithm for thermoacoustic and photoacoustic tomography with variable sound speed. *SIAM J. Imaging Sci.*, 4(3):850–883, 2011.
- [Sch11] O. Scherzer (Editor) (2011) “*Handbook of Mathematical Methods in Imaging*” (Springer).
- [SU09] P. Stefanov and G. Uhlmann. Thermoacoustic tomography with variable sound speed. *Inverse Problems*, 25(7):075011, 16, 2009.
- [SU11] P. Stefanov and G. Uhlmann. Thermoacoustic tomography arising in brain imaging. *Inverse Problems*, 27(4):045004, 26, 2011.
- [SY15] P. Stefanov and Y. Yang. Multiwave tomography in a closed domain: averaged sharp time reversal. *Inverse Problems*, 31(6):065007, 2015.
- [XW05] M. Xu and L. Wang 2005 Universal back-projection algorithm for photoacoustic computed tomography *Phys. Rev. E* **71** 016706
- [XW06] M. Xu and L. Wang. Photoacoustic imaging in biomedicine. *Review in Scientific Instruments*, 77(041101), 2006.